A numerical assessment of the influence of compaction on the seismic performance of Geosynthetic-Reinforced Earth retaining walls

Domenico Gaudio[1*], *Ludovica* Cioffi[1], and *Luca* Masini[1]

[1]Department of Structural and Geotechnical Engineering, Sapienza Università di Roma, via Eudossiana 18, 00184, Rome, Italy

Abstract. Over the past three decades, field observations have demonstrated the resilience of Geosynthetic-Reinforced Earth (GRE) retaining walls to severe earthquakes. Seismic damage to GRE walls generally manifests as permanent deformations due to the transient activation of plastic mechanisms within the soil-reinforcement system, demonstrating their overall ductile behaviour. However, a limited understanding of the reinforcement-soil interactions under static and dynamic conditions and the lack of specific guidelines in many building codes for the seismic design of GRE walls have hindered their widespread adoption. In particular, the design parameters for both the backfill and the mechanical properties of the reinforcement are usually selected according to an overly conservative approach which neglects the effects of high compaction energy. As a result, a GRE wall in a well compacted granular soil is often designed with a soil shear strength that is much lower than the strength available. This paper discusses the effects of compaction on the initial stress and strain distribution in the reinforcement and their impact on the seismic performance of GRE walls. To this end, iterative pseudo-static and dynamic time-domain numerical analyses were carried out to assess how compaction affects both the plastic mechanisms and the seismic performance of reinforced soil walls.

1 Introduction

Selection of the strength parameters of the soil between the reinforcements to adopt in the seismic design of GRE walls is still a controversial issue amongst the codes available worldwide. Best practice requires that the coarse-grained soil used in the reinforced zone is adequately compacted: it follows that, for the typical heights of the GRE walls, such soil mobilises a higher peak shear strength angle than that at constant volume, depending on the confining stress level. This observation is corroborated by the experimental results obtained by Zornberg (2002) [1] from geotechnical centrifuge tests, which showed that the shear strength mobilised is the one at peak. It is therefore reasonable to assume that the

* Corresponding author: domenico.gaudio@uniroma.1.it

© The Authors, published by EDP Sciences. This is an open access article distributed under the terms of the Creative Commons Attribution License 4.0 (https://creativecommons.org/licenses/by/4.0/).

characteristics of the plastic mechanisms activated in the reinforced soil during intense seismic events is also related to peak conditions.

However, the need to ensure a global ductile behaviour of the structure [2], in which the system activates plastic mechanisms and accumulates irreversible displacements in the presence of exceptional loads (such as an earthquake), without losing the necessary safety or functional requirements, has led many design guidelines to adopt strength characteristics of the reinforced soil that are more representative of the shear strength at constant volume, regardless of the degree of soil compaction. This assumption would therefore lead to an overly cautious design of the structure for static actions. In this respect, one option may be to assume a shear strength angle that varies with depth within the structure [3]. Hybrid global limit equilibrium methods have also been proposed in the literature [4], in which the plastic mechanism is determined by considering peak conditions, while the reinforcement length and tensile load are evaluated by considering that progressive failure phenomena reduce the shear strength to constant volume conditions.

With regard to the choice of shear strength parameters under seismic conditions to be used in analyses performed with pseudostatic or simplified Newmark's methods, it is generally recommended to refer to the constant-volume shear strength (*e.g.* [5]) to ensure a certain degree of overstrength and overall ductile behaviour of the system.

This paper presents some preliminary results of a study aimed at evaluating the effects of compaction on the distribution of the initial stress and strain state in the backfill soil, and on the subsequent seismic behaviour of the reinforcement-soil system. To this end, iterative pseudo-static and dynamic numerical analyses were conducted, in which the shear strength of the backfill is described by a friction angle that depends on the mean effective stress. The results are compared with those obtained by assuming a constant value for the shear strength angle of the embankment, which is more representative of a constant volume condition.

2 Static conditions

To assess the effect of backfill shear strength on the seismic performance of reinforced earth walls, a numerical analysis was performed under plane-strain conditions with the numerical model implemented by Masini *et al.* (2015) [6] in the Finite Difference (FD) code FLAC v. 7.0 [7]. The analyses were performed referring to the problem layout depicted in Figure 1. Specifically, a reinforced earth wall of height $H = 15$ m, with $n = 25$ uniformly spaced reinforcement levels (constant spacing of the reinforcement layers $s = 0.6$ m) and equal length $B = 11.25$ m ($B/H = 0.75$) was considered; the wall facing is inclined at an angle $\beta = 80°$ to the horizontal. The porewater pressures are zero, assuming the drainage system placed at the rear of the wall to work properly. A unit volume weight $\gamma = 20$ kN/m^3 and a Mohr-Coulomb failure criterion were assumed for all soils. Specifically, for the foundation soil, strength parameters representative of a medium fine-grained le material were adopted ($\varphi' = 28°$ and $c' = 10$ kPa), while for the backfill a purely frictional criterion ($c' = 0$) was adopted, with the shear strength angle φ' depending on the mean effective stress p' and the relative density D_R, according to the renowned equation proposed by Bolton (1986) [8]:

$$\varphi' - \varphi'_{cv} = m \cdot \left[D_R \left(10 - \ln p'\right) - 1 \right] \quad (1)$$

where m is a coefficient which depends on the testing deformation conditions ($m = 3$ in axisymmetric conditions, $m = 5$ in plane-strain conditions). In particular, reference has been made to a material consisting of a mixture of 70% Ticino sand (TS) (e.g.: [9] and [10]) and 30% Pontida clay (PON). Ventini *et al*. (2021) [11] reported the results of several laboratory tests to evaluate the physical, mechanical, and hydraulic properties of the mixture, carried

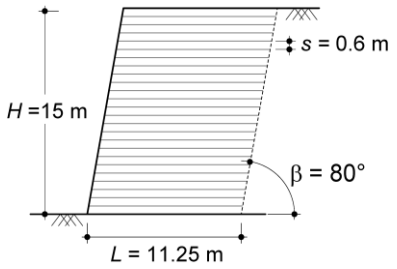

Fig. 1. Problem layout.

Table 1. Physical and mechanical properties of the 70% TS–30% PON mixture [11].

γ_d (kN/m^3)	w (%)	e (-)	S_r (%)	e_{min} (-)	e_{max} (-)	φ'_{cv} (°)
20.97	7.61	0.256	79.92	0.236	0.953	33

out under fully and partially saturated conditions (Table 1). The dry unit weight γ_d, the water content w, the void ratio e and the degree of saturation S_r were obtained from compaction tests carried out at the optimum moisture content of the modified Proctor standard. The critical state shear strength angle φ'_{cv} was obtained from consolidated drained triaxial (TX-CID) tests. In terms of grain size, the 70% TS - 30% PON mixture can be classified as a low plasticity silty sand.

In the analyses it was assumed that the embankment material was placed and compacted to 95% of the Proctor optimum in terms of dry unit weight γ_d, which corresponds to a void ratio $e = 0.322$ and a relative density $D_R = 88\%$, the latter calculated with the e_{min} and e_{max} values reported in Table 1.

The elastic field behaviour of both soils is defined by a tangential elasticity modulus G, a function of the mean effective stress p', which is updated at the end of each construction phase:

$$\frac{G}{p_r} = A \cdot \left(\frac{G_0}{p_r} \right) = A \cdot \left(B + C \cdot \left(\frac{p'}{p_r} \right)^D \right) \tag{2}$$

where G_0 is the small-strain shear modulus, A, B, C and D are dimensionless stiffness parameters which are listed in Table 2 and $p_r = 1$ kPa is a reference pressure introduced so that equation (2) is dimensionless. The deformable facing of the GRS wall was simulated by two zone columns with elastic behaviour and stiffness equal to that of the backfill.

The reinforcement layers were modelled using the *strip* structural elements available in the FD code, which are only capable of transferring axial tensile loads. The axial strain ε and the tensile load per unit width T are linked through a linear elastic-perfectly plastic constitutive model, with an axial stiffness $EA = 1250$ kN/m and a tensile strength $T_T = 25$ kN/m. The reinforcement layers are assumed to be infinitely ductile, starting from the yield axial strain, $\varepsilon_y = 2\%$.

The behaviour at the soil-reinforcement interface is elastic-perfectly plastic, with a Mohr-Coulomb failure criterion, a zero cohesion and a shear strength angle $\varphi'_{s/GSY} = \tan^{-1}(f_{s/GSY} \cdot \tan \varphi')$, where $f_{s/GSY}$ is a reduction factor of the interface resistance and φ' is the shear strength angle of the soil in contact with the reinforcement. In the analyses, $f_{s/GSY} = 1$ was assumed, in accordance with Masini *et al.* (2015) [6]. The tangential stiffness

Table 2. Shear strength and stiffness parameters.

soil	c' (kPa)	φ' (°)	A (-)	B (-)	C (-)	D (-)
backfill	1	variable	0.500	5100	5329.5	0.500
found. soil	10	28	0.132	12750	1397.4	0.790

of the interface was calibrated to mobilise the resistance for very small displacements, *i.e.*, of the order of magnitude of mm.

The FD mesh (not shown here for brevity) is composed of 180 by 135 quadrangular zones. Standard fixities (*i.e.*, bottom boundary fully fixed, side boundaries only horizontally fixed) have been applied to the boundary of the mesh during the static stages. The calculation phases defined in the analyses consist of an initial phase in which the lithostatic stress state is generated, followed by 25 construction phases of the wall and backfill. Each construction stage includes the activation of a reinforcement layer, the corresponding section of the façade and a 60 cm layer of backfill. Due to the change in effective stresses induced by the construction phase, at the end of each phase the soil stiffness is updated using Eq. (1) and the shear strength angle of the backfill is recalculated using Bolton's equation [8].

Figure 2 shows the contour lines of the shear resistance angle φ' (Fig. 2a) at the end of the construction phases, together with the profiles of the dimensionless tensile axial strain, $\varepsilon/\varepsilon_y$, and load in the reinforcement layers, T/T_T (Fig. 2b). The progressive mobilisation of the shear resistance of the backfill during the construction phases is characterised by a markedly uneven distribution of the shear strength angle in the reinforced zone (Fig. 2a). In the upper part of the wall, characterised by lower mean effective stress values, the difference $\varphi'-\varphi'_{cv}$ was limited to 12° [8]: under these circumstances, all reinforcement levels fall in their elastic regime ($\varepsilon/\varepsilon_y$ and $T/T_T < 1$), except for the bottom layer (Fig. 2b).

3 Pseudostatic analyses

Starting from the last construction phase of the wall, the critical seismic coefficient k_c and the associated plastic mechanism were iteratively searched by means of a pseudostatic

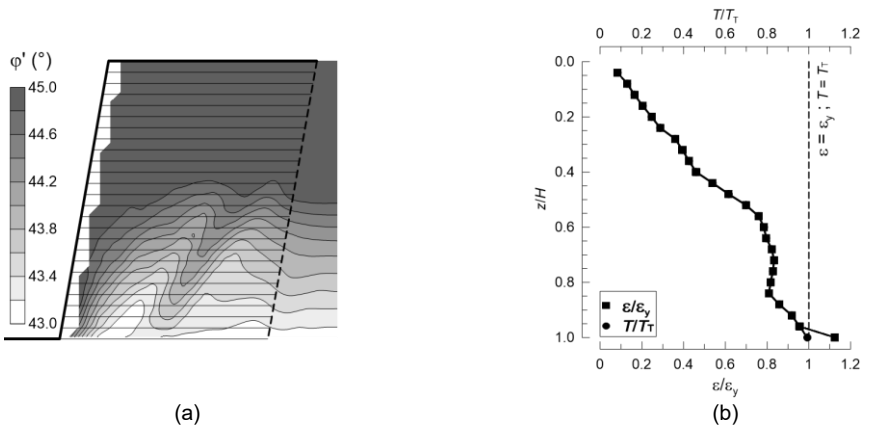

Fig. 2. End of the construction phases: (a) contours of the mobilised shear strength angle; (b) profiles of the dimensionless tensile axial strain and load in the reinforcement layers.

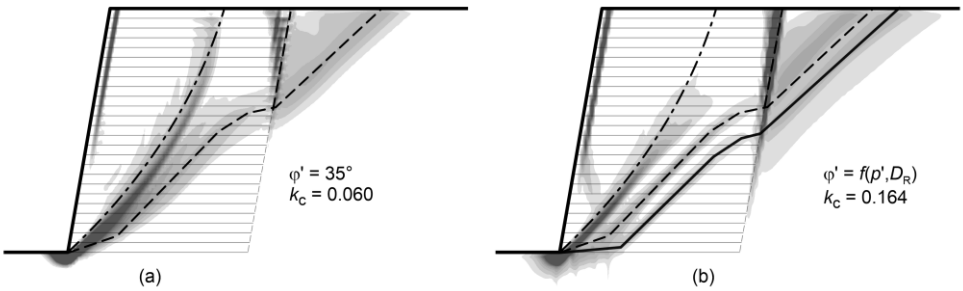

Fig. 3. Pseudostatic numerical analyses. Contour lines of shear strain γ/2: a) constant shear strength angle [9] b) variable shear strength angle.

numerical analysis, in which the horizontal component of the inertial forces $k_h \cdot \gamma/g$ was progressively increased. The critical seismic coefficient, k_c, is therefore the value of k_h at which the system accumulates displacements without the calculation algorithm being able to achieve convergence. Consequently, the specific values of displacements and strains obtained do not have a direct physical meaning, since they refer to a condition in which the system is not in equilibrium and is therefore accelerating.

Figure 3 shows the contour lines of the shear strain $\varepsilon_{xy} = \gamma/2$ obtained for $k_h = k_c$. In particular, Figure 3a shows the results obtained by Masini *et al*. (2015) [6] for φ' = 35°, while Figure 3b refers to the case where the shear resistance angle varies with the mean effective stress. In the same figure, the plastic mechanisms identified by the isolines of γ/2 are highlighted. In both cases, a band of highly deformed soil propagates from the base of the wall, progressively intersecting the reinforcement levels, according to a rotational mechanism within the wall. At the same time, a second mechanism develops towards the rear of the reinforced zone, which can be interpreted as a two-block mechanism, one outside the reinforcements and one inside them. For this mechanism, some reinforcement levels located in the upper part of the wall are included in the plastic volume. The results of the numerical analysis therefore indicate that two plastic mechanisms develop at the limit conditions: a main plastic mechanism, of mixed type and partially external to the reinforced zone, and a secondary plastic mechanism, internal to the reinforced zone. To the aforementioned mechanisms, a third one is added in the case of a variable shear resistance angle (continuous line in Fig. 3b): this mechanism is similar to the previously discussed two-block mechanism but is located farther outward from the wall.

The identification of the seismic resistance of the system and the corresponding plastic mechanisms provides a better understanding of the effect of compaction on the seismic performance of the wall. It is also worth noting that the seismic resistance and collapse mechanisms are properties of the system, depending on the geometry and the mechanical resistance characteristics of the structure. Therefore, they are independent of the seismic input, as discussed in the following.

4 Dynamic analyses

The deformation patterns resulting from the pseudostatic analyses were compared with the dynamic response of the GRS wall by performing time-domain dynamic analyses in which a time history of the horizontal acceleration was applied to the bottom boundary. Therefore, at the end of the static phases of the wall construction, the static boundary conditions were removed and the boundary conditions relative to the dynamic calculation phase were applied. Specifically, free field conditions were applied to the vertical boundaries (*free-field* constraints), capable of absorbing the waves propagating outside the domain; the North-

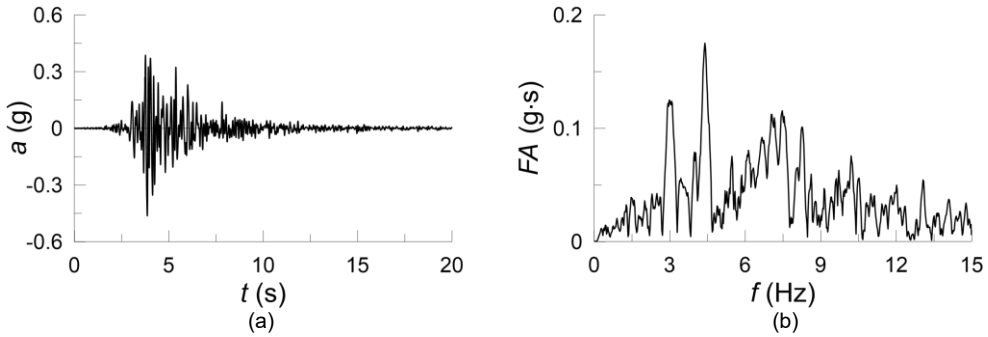

Fig. 4. N-S- Monte Cavallo seismic input: a) horizontal acceleration time history; b) Fourier amplitude spectrum.

South seismic record of the Monte Cavallo earthquake (Central Italy Earthquake, 2016) was applied to the bottom boundary of the numerical model. The acceleration time history was characterised by a maximum acceleration $a_{max} = 0.46g$, an Arias intensity $I_a = 1.17$ m/s, a predominant frequency $f_p = 4.40$ Hz, and a significant duration $D_{5\text{-}95} = 4.23$ s, after being low-pass filtered at $f_{max} = 15$ Hz and baseline corrected with a second-order parabola. The relevant horizontal acceleration time history and Fourier amplitude spectrum are plotted in Figure 4. The vertical component of the velocity of the lower boundary nodes was assumed to be zero. The calculation time step used for the explicit algorithm is 10^{-6} s.

The dynamic behaviour of the soil was described by the hysteretic model *Sig3*, available in FLAC 7.0 library, where the relation between the shear stress τ and the corresponding shear strain γ is expressed by the relation:

$$\frac{\tau}{G_0} = \bar{\tau} = \frac{G_s(\gamma)}{G_0} \cdot \gamma = M_s(\gamma) \cdot \gamma \tag{3}$$

where $G_s(\gamma)$ is the secant shear modulus as a function of strain γ; G_0 is the small-strain shear modulus, $\bar{\tau}$ and M_s are the normalised shear stress and shear modulus. The relationship between M_s and γ represents the decay curve of the shear modulus and is expressed by the equation:

$$M_S = \frac{a}{1 + e^{-\frac{\log\gamma(\%) - x_0}{b}}} \tag{4}$$

where the parameters a, b and x_0 can be calibrated from experimentally obtained modulus decay curves. In particular, reference has been made to the curve proposed by Seed & Idriss (1970) [12] for coarse-grained materials, which can be described by equation (4) assuming $a = 1.014$, $b = -0.4792$, $x_0 = -1.249$. In the model, the unloading and reloading behaviour is described by a generalisation of the Masing rules to a two-dimensional strain state. This results in a hysteretic behaviour that produces an energy dissipation proportional to the maximum cyclic strain. In addition to the hysteretic damping, the model can reproduce an additional source of energy dissipation associated with the development of plastic deformations as soil strength is mobilised. Additional Rayleigh viscous damping was also used in the analyses to improve the numerical stability of the analyses. For this purpose, a minimum damping ratio $\xi_{min} = 4\%$ was used at the fundamental frequency of the deposit, equal to $f_0 = 1.75$ Hz.

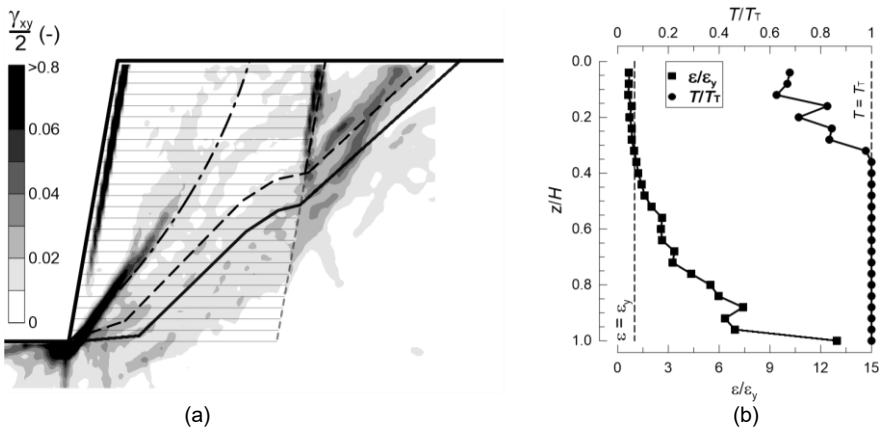

Fig. 5. End of the dynamic calculation phase: a) contours of permanent shear strains; b) profiles of the dimensionless tensile axial strain and load in the reinforcement layers.

Figure 5 shows the main results obtained at the end of the earthquake for the wall with a variable angle of shear strength, such as the contour lines of shear deformation (Fig. 5a) and the profile of the axial deformation of the reinforcement elements, ε, and the corresponding tensile force, T, normalized with respect to the yield strain, ε_y, and the tensile strength, T/T_T (Fig. 5b). From the large values of the strains attained, it is immediately evident that the intensity of the seismic input is sufficient to activate the plastic mechanisms of the system. This result was somewhat expected, since the maximum seismic coefficient of the input accelerogram, $k_{max} = a_{max}/g = 0.46$, is significantly higher than the system critical seismic coefficient, $k_c = 0.164$. Furthermore, the plastic mechanisms activated during the seismic event are consistent with those previously obtained from the pseudo-static analysis, providing further confirmation that collapse kinematics are a property of the system, independent of the seismic motion properties, provided that the input intensity is large enough to activate these mechanisms. However, the largest shear strains are obtained for the two-block mechanisms, where the reinforcement elements located in the upper part of the wall ($z/H < 0.3$ in Fig. 5b) are fully incorporated into the mechanism and thus unable to contribute to stabilise the structure. In contrast, the reinforcement elements positioned in the lower part of the wall ($z/H > 0.3$ in Fig. 5b) exhibit an anchoring length, or effective length, sufficient to ensure the resisting contribution. Consistent with these observations, the profiles shown in Figure 5b illustrate that approximately 30% of the reinforcements ($z/H < 0.3$) remain in the elastic range ($\varepsilon/\varepsilon_y < 1$, $T/T_T < 1$), while the remaining 70% ($z/H > 0.3$) yield ($\varepsilon/\varepsilon_y \geq 1$) and, consequently, attain their tensile strength ($T/T_T = 1$) during the seismic event.

The results previously discussed regarding the pseudo-static and dynamic conditions are corroborated by the time histories of the horizontal displacement of the wall crest (u) relative to the free-field horizontal displacement (u_{FF}) measured at ground surface, as shown in Figure 6. These time histories are presented for both cases considered in the study: one in which the beneficial effects of compaction of the soil between the reinforcement elements are neglected ($\varphi' = \text{const.} = 35°$, close to $\varphi'_{cv} = 33°$) and the other where these effects are explicitly accounted for ($\varphi' = f(p', D_R) = 43°$ to 45°). The displacements accumulated when neglecting the effects of compaction are significantly higher than those calculated when such effects are considered, for the entire duration of the earthquake: permanent values at the end of the seismic event were found to be approximately $u - u_{FF} = 1.28$ m and 0.25 m in the two cases, respectively. This significant difference is primarily attributable to the different seismic resistance of the two systems, here expressed by the critical seismic coefficient, $k_c = 0.060$ and 0.164, in the absence and the presence of compaction effects, respectively. It is also worth

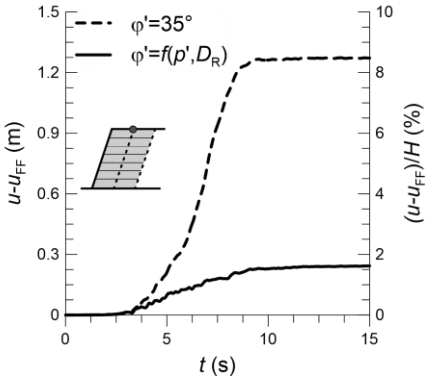

Fig. 6. Time history of the horizontal displacement of the wall crest relative to the free field.

noting that the effect of compaction is limited to increasing the friction angle of the soil from 33 to 45°, which explains the gain in the seismic resistance found and the relevant seismic performance.

In the framework of a Performance-Based Design (PBD) approach, the seismic performance of the two systems can be expressed in terms of an index, such as the permanent relative displacement at the end of the earthquake normalized with respect to the wall height, $(u - u_{FF})/H$. This performance index is approximately equal to 8.5% in the absence of compaction, while it is about 1.7% in the presence of the compaction effects, the former value clearly corresponding to collapse of the wall. Indeed, with reference to the displacement threshold values identified by Huang *et al*. (2009) [13], equal to 2% to 5%, the lower limit representing moderate and acceptable displacement, the upper limit indicating catastrophic damage to the structure, it is apparent that the seismic performance of the wall without compaction effects would be judged largely insufficient, whereas the compaction effects would bring the seismic performance close to be acceptable. Such a difference in the seismic performance assessment of the two walls confirms the need to account for the effects of the construction phases of the reinforced earth wall, otherwise the seismic performance assessment would be overly conservative, this adversely affecting both the cost and environmental impact of the structure.

It is worth emphasising that the seismic performance evaluation of the two cases considered in this study is influenced by the simplifying assumptions underlying the numerical analyses. Specifically, it is evident that the constitutive model selected for the soil used in the reinforced earth structure does not capture the negative hardening associated with the progressive accumulation of deformation (strain-softening), as typically observed in compacted coarse-grained soils with a high relative density (D_R = 88%). In this regard, it is important to note that Huang *et al*. (2009) [13] experimentally observed through shake table tests that the peak shear resistance angle is maintained for a normalized horizontal displacement below the aforementioned 2% threshold, while reaching the 5% threshold corresponds to the post-peak or even constant-volume conditions. The constitutive assumptions underlying this study regarding the soil mechanical behaviour align with these experimental observations. Specifically, for the wall with φ' = const. = 35°, close to φ'_{cv} = 33°, a maximum displacement far beyond the threshold of 5% was calculated, whereas for the case with φ' = $f(p', D_R)$ a maximum displacement below 2% was obtained.

5 Conclusions

In the design of GRE retaining walls, the choice of the strength parameters to be adopted for the reinforced soil remains a topic of debate. Typically, the chosen value, for safety reasons, corresponds to the constant-volume friction angle, thereby neglecting the beneficial effect of densification induced by the soil compaction between the reinforcements. This design assumption leads to excessive conservatism in the design of GRE retaining walls in seismic areas, to the detriment of both the cost and the environmental impact of the structure.

In this paper, the resistance and seismic performances of a reinforced earth wall subjected to an intense seismic event were compared under two hypotheses, namely the presence and the absence of soil densification due to compaction. The aim of the study was to highlight the effects of the increase in shear strength due to backfill compaction on the seismic resistance of the retaining wall. In this preliminary stage of the research, soil dilatancy was neglected and the reinforcement was considered to be infinitely ductile. The results were obtained by performing iterative pseudo-static analyses and nonlinear dynamic analyses under plane strain conditions using the Finite Difference method. The findings demonstrated that soil compaction significantly increases the seismic resistance of the system, here represented by the critical seismic coefficient k_c, and leads to a corresponding improvement in the seismic performance of the wall. The performance is described in terms of a performance index, defined as the permanent horizontal displacement of the wall crest relative to free-field conditions and normalized by the wall height. Finally, the seismic performance evaluation thus obtained was conducted by comparing the performance index with threshold values reported in the literature and commonly adopted in professional practice.

References

1. J. G. Zornberg, Peak versus residual shear strength in geosynthetic-reinforced soil design. Geosynth. Int. **9**(4), 301–317 (2002) https://doi.org/10.1680/gein.9.0220
2. D. Gaudio, L. Masini, S. Rampello, A performance-based approach to design reinforced-earth retaining walls. Geotext. Geomembr. **46**(4), 470-485 (2018) https://doi.org/10.1016/j.geotexmem.2018.04.003
3. N. Moraci, Il rinforzo dei terreni con geosintetici: recenti sviluppi tecnologici, progettuali, in Proceedings of the XXIV Convegno Nazionale di Geotecnica, Napoli, Italy, 22-24 Giugno, Associazione Geotecnica Italiana, Vol. 1, 149-198 (2011) (in Italian)
4. D. Leshchinsky, Design Dilemma: Use peak or residual strength of soil. Geotext. Geomembr. **19**, 111-125 (2001) https://doi.org/10.1016/S0266-1144(00)00007-8
5. H. Liu, H. Ling, Seismic Responses of Reinforced Soil Retaining Walls and the Strain Softening of Backfill Soils. Int J Geomech **12**(4), 351-356 (2012).
6. L. Masini, L. Callisto, S. Rampello, An interpretation of the seismic behaviour of reinforced-earth retaining structures. Géotechnique **65**(6), 349-358 (2015) https://doi.org/10.1680/geot.SIP.15.P.001
7. Itasca, FLAC Fast Lagrangian Analysis of Continua v. 7.0. User's Manual. Minneapolis, MN: Itasca Consulting Group (2011).
8. M. D. Bolton, The strength and dilatancy of sands. Géotechnique **36**(1), 65-78 (1986) https://doi.org/10.1680/geot.1986.36.1.65

9. R. Bellotti, M. Jamiolkowski, D.C.F Lo Presti, D.A O'Neill, Anisotropy of small strain stiffness in Ticino sand. Géotechnique **46**(1), 115–131 (1996) https://doi.org/10.1680/geot.1996.46.1.115
10. V. Fioravante, D. Giretti, Unidirectional cyclic resistance of Ticino and Toyoura sands from centrifuge cone penetration tests. Acta Geotech. **1**1, 953–968 (2016) https://doi.org/10.1007/s11440-015-0419-3
11. R. Ventini, E. Dodaro, C.G. Gragnano, D. Giretti, M. Pirone, Experimental and numerical investigations of a river embankment model under transient seepage conditions. Geosciences **11**(5), 192 (2021) https://dx.doi.org/10.3390/geosciences11050192
12. H. B. Seed, I. M. Idriss, Soil moduli and damping factors for dynamic response analyses. Report No. EERC 70-10, Earthquake Engineering Research Center, Univ. of California, Berkeley, Calif (1970)
13. C. C. Huang, S. H. Wu, H. J. Wu, Seismic displacement criterion for soil retaining walls based on soil strength mobilization. J. Geotech. Geoenviron. Eng. **135**(1), 74-83 (2009) https://doi.org/10.1061/(ASCE)1090-0241(2009)135:1(74)